Probing the tunability of magnetism with external pressure in metastable Sr$_2$NiIrO$_6$ double perovskite

M. A. Laguna-Marco [1,2,*] E. Arias-Egido [1,2] V. Cuartero [1,3] J. Herrero-Albillos [1,3] P. Kayser [4] J. A. Alonso [4] G. Fabbris [5] D. Haskel [5] and T. Irifune [6,7]

[1]*Instituto de Nanociencia y Materiales de Aragón, CSIC - Universidad de Zaragoza, Zaragoza 50009, Spain*
[2]*Departamento de Física de la Materia Condensada, Universidad de Zaragoza, Zaragoza 50009, Spain*
[3]*Departamento de Ciencia y Tecnología de Materiales y Fluidos, Universidad de Zaragoza, Zaragoza 50018, Spain*
[4]*Instituto de Ciencia de Materiales de Madrid, CSIC, Cantoblanco 28049 Madrid, Spain*
[5]*Advanced Photon Source, Argonne National Laboratory, Argonne, Ilinois 60439, USA*
[6]*Geodynamics Research Center, Ehime University, 2-5 Bunkyo-cho, Matsuyama 790-8577, Japan*
[7]*Earth-Life Science Institute, Tokyo Institute of Technology, Tokyo 152-8500, Japan*

In Sr$_2$NiIrO$_6$ long-range Ir-Ir antiferromagnetic exchange interactions have been reported to overcome the ferromagnetic Ni-Ir interactions hampering the otherwise expected ferromagnetic behavior. Prompted by this, a combination of x-ray absorption spectroscopy and x-ray diffraction at high pressure is used here to investigate the interplay between the magnetic structure of the Ir sublattice and lattice degrees of freedom. The compression of Sr$_2$NiIrO$_6$ drives an unexpected nonmonotonic change of the x-ray magnetic circular dichroism (XMCD) spectra: The intensity first decreases in the 0- to 18-GPa range, then shows an increase in the 18- to 30-GPa range and again decreases for higher pressures. The XMCD intensity, a measure of the net magnetization in the Ir sublattice, however, is found to remain very low in the whole pressure range so the observed changes do not correspond with a transition from antiferromagnetic to ferromagnetic or ferrimagnetic order. The evolution of the XMCD is better explained in terms of a weakening/strengthening of the long-range antiferromagnetic (AFM) Ir-Ir interaction between ferromagnetic planes associated with the reduction of the lattice parameters. In particular, a correlation can be established between the evolution of the b/a ratio and the weakening/strengthening of the AFM interaction.

I. INTRODUCTION

Iridium-based oxides are lately attracting a lot of attention in material science [1–3]. Among them, the versatility afforded in ordered double perovskites A$_2$BIrO$_6$ provides a prolific playground for exploration of novel electronic and magnetic properties. Combinations of magnetic 3d metals and Ir are particularly promising: The localized 3d electrons provide strong local magnetic moments, while the more delocalized 5d electrons of Ir and their strong spin-orbit coupling can be a source of high magnetic ordering temperatures and enhanced anisotropy [4–8]. The extended 5d orbitals may result in large overlaps and strongly structure-dependent interactions. Therefore, one may expect that, as a result of the large spatial extent of 5d wave functions, it will be feasible to tune their electric and magnetic properties by external stimuli, such as high pressure (HP). Among A$_2$BIrO$_6$ compounds, high oxidation iridates (Ir^{6+}) may be especially interesting because the covalence of the Ir-O chemical bonds is correlated with the value of the magnetic ordering temperature, which makes them especially relevant for practical spintronic applications.

In order to tailor the behavior of these materials we need first to understand the local moments and exchange interactions from which their magnetic properties are derived. However, the prediction of the behavior of the double perovskites containing Ir (and 5d transition metal ions in general) is far from being achieved. While the mechanisms regulating 3d-3d exchange interactions are rather well understood, the understanding of 5d-5d and 3d-5d interactions is much less developed. The observed 3d-5d coupling often violates the Goodenough-Kanamori (GK) rules [9,10] when 5d ions are present. Recent works point out that the presence of extended 5d orbitals may require accounting for longer-range exchange pathways beyond first neighbor exchange in order to understand magnetic phenomena [5,11–15]. In this respect, recent works on Sr$_{2-x}$Ca$_x$FeOsO$_6$ suggest that the remarkable modification of the magnetic response with chemical pressure is related to the Os 5d orbitals [13]. Similarly, exchange between 5d next nearest neighbors is found to be key in the behavior of Ca$_2$NiOsO$_6$ and Ca$_2$CoOsO$_6$ [12]. In addition, these works suggest that these competing magnetic superexchange interactions are highly sensitive to changes in the B-O-B′ bond angles [13].

In this context, the magnetic behavior reported for Sr$_2$NiIrO$_6$ is especially interesting. According to GK rules (Sr$_2$NiIrO$_6$ is insulating and thus its magnetic properties are mainly dictated by superexchange interactions), one would expect a ferromagnetic (FM) behavior based on the FM coupling between the Ni^{2+} (t$_{2g}^6$e$_g^2$) and Ir^{6+} (t$_{2g}^3$) ions, but

*anlaguna@unizar.es

the magnetization and magnetic susceptibility measurements show the establishment of antiferromagnetic (AFM) interactions at $T_N \sim 58$ K [16]. Moreover, density functional calculations indicated that the Ir-Ir interaction is AFM and slightly stronger than the Ir-Ni FM one [14]. Based on this, the authors proposed that the competing interactions would result in a distorted low-temperature AFM, probably type III. A more recent neutron diffraction study, however, has revealed a complex incommensurate helical magnetic order [15].

The similar magnetization behavior observed in Sr_2NiIrO_6 and Sr_2BIrO_6 perovskites with nonmagnetic B ions, such as Sr_2ZnIrO_6, points out that the Ir-Ir may be the more important interaction to understand the magnetic behavior of Ir double perovskites. On the other hand, the frustration index f_{frus}, defined as $f_{frus} = |\Theta_{Weiss}|/T_N$, is 9.5 for Sr_2ZnIrO_6 [16], while it only reaches 1.4 for Sr_2NiIrO_6 [15]. This suggests an additional key role of the Ir-Ni interaction in stabilizing the observed magnetic structure.

All this points out the potentially tunable magnetism of the Sr_2NiIrO_6 compound and makes it a particularly appropriate system to shed light into both the local Ir magnetic moment and the magnetic interactions defining the magnetic properties. In relation to the value of the local (atomic) magnetic moment of Ir, it should be noted that, to the best of our knowledge, neither FM nor ferrimagnetic (FiM) structure has been reported yet for any Ir oxide. For AFM systems (typically canted AFM), disparate values have been reported for the Ir magnetic moment [16–23], likely associated with the difficult detection of Ir magnetic moment by the typically used neutron powder diffraction technique. In this work we propose a combined HP-XRD, HP-EXAFS, and HP-XMCD study of Sr_2NiIrO_6 oxide to get further insight into these questions. Demanding high-pressure experiments are used to explore to what extent the sensibility of the $5d$-$5d$ and $3d$-$5d$ interactions to structural changes (can) lead to significant changes in the magnetic structure. In order to better disentangle the contribution of $5d$-$5d$ and $3d$-$5d$ interactions, Sr_2ZnIrO_6 is also included in our study.

II. EXPERIMENTAL

Polycrystalline Sr_2ZnIrO_6 and Sr_2NiIrO_6 samples were prepared via the citrate-nitrate method and subsequently annealed in an oxidizing atmosphere between 900 °C–1100 °C to obtain the pure compounds. Further details of the preparation method can be found in Ref. [16].

Basic structural characterization at ambient pressure can be found in Ref. [16]. High pressure x-ray diffraction (HP-XRD) measurements were carried out at the 16-BM-D beamline of the Advanced Photon Source (APS), Argonne National Laboratory (ANL). HP-XRD data were recorded at $T = 10$ K and under pressures up to 50 GPa. Fine powder was loaded into the sample chamber ($\sim$90-μm hole in a Re gasket preindented to 30 μm) together with He gas as the quasihydrostatic pressure medium and a couple of ruby spheres and gold grains as the *in situ* pressure calibrants. A symmetric diamond anvil cell (DAC, Princeton) with 300-μm culet anvils was used for these measurements. Data were collected using x-ray radiation with $\lambda = 0.4016$ Å (30.87 keV) and a MAR345 image plate. The two-dimensional diffractograms were integrated using the

DIOPTAS software [24]. The one-dimensional (1D) patterns were profile matched using the FULLPROF code [25].

The EXAFS spectra at the Ir L_3 absorption edge were recorded under applied high pressures (2.5–50 GPa) and at low temperature (10 K) at the ID24 [26] beamline of the ESRF (Grenoble, France). ID24 energy dispersive spectrometer was used to perform the EXAFS measurements. The measurements were also performed in transmission by using a one-dimensional Hamamatsu CCD camera. We used nanopolycrystalline diamond anvils [27] to avoid glitches (i.e., strong Bragg peaks) from the anvils on the EXAFS spectra. Ruby chips were used as pressure markers and Ne gas was used as pressure transmitting medium. The EXAFS spectra were analyzed according to standard procedures [28] using the HORAE-IFEFFIT (ATHENA, ARTEMIS) program package [29,30]. For the analysis of the EXAFS spectra at the Ir L_3 edge, a cluster 7 Å in size was used in calculating theoretical standards [31]. EXAFS data in the 2.5- to 9.4-Å^{-1} k range (Hanning window, $dk = 0.5$ Å^{-1}) were Fourier transformed and fitted in real space.

The XANES/XMCD measurements under high pressure were carried out at beamline 4-ID-D of the Advanced Photon Source, Argonne National Laboratory. The spectra were recorded at the Ir $L_{2,3}$ absorption edges ($2p_{\frac{1}{2},\frac{3}{2}} \rightarrow 5d$ transition) to probe the Ir $5d$ states. Circularly polarized x rays were generated using phase-retarding optics [32,33]. Harmonic rejection was achieved by the combined effects of x-ray reflection from two Pd mirrors at 3.1 mrad incidence angle and detuning of the second crystal in the Si(111) double crystal monochromator. XMCD was measured by switching x-ray helicity (13.1 Hz) and detecting the related modulation in absorption coefficient with a lock-in amplifier [34]. All the measurements were done in transmission geometry, at low temperature (10-K range) and under a magnetic field of 3.5 T applied along the x-ray propagation direction. For the high pressure measurements the powdered samples were loaded on copper-beryllium DACs fitted with 300-μm culet anvils and a Re gasket [35]. Ne gas was used as the quasihydrostatic pressure transmitting medium and ruby powder for *in situ* pressure calibration. The samples were cooled in ^{4}He vapor using the variable temperature insert of the superconducting magnet, and pressure was controlled remotely using a He-gas membrane.

III. RESULTS AND DISCUSSION

A. Magnetic characterization

As can be seen in Figs. 1(a) and 1(b), the XMCD signal of Sr_2NiIrO_6 shows an unusual nonmonotonic dependence on hydrostatic pressure. In particular, the XMCD intensity first undergoes a reduction along the 0- to 18-GPa range. Above 18 GPa, a continuous increase in XMCD signal is observed with increasing pressure reaching twice its ambient pressure value at $\sim$30 GPa. For higher pressures the intensity starts to decrease again. The same pressure dependence is observed at both edges, indicating that the changes are not related to a change in L_z/S_z ratio. Despite the increase observed in the 18- to 30-GPa range, the intensity of the XMCD spectra is always very low. XMCD < 0.025 (0.015) at the L_2 (L_3) edge is found
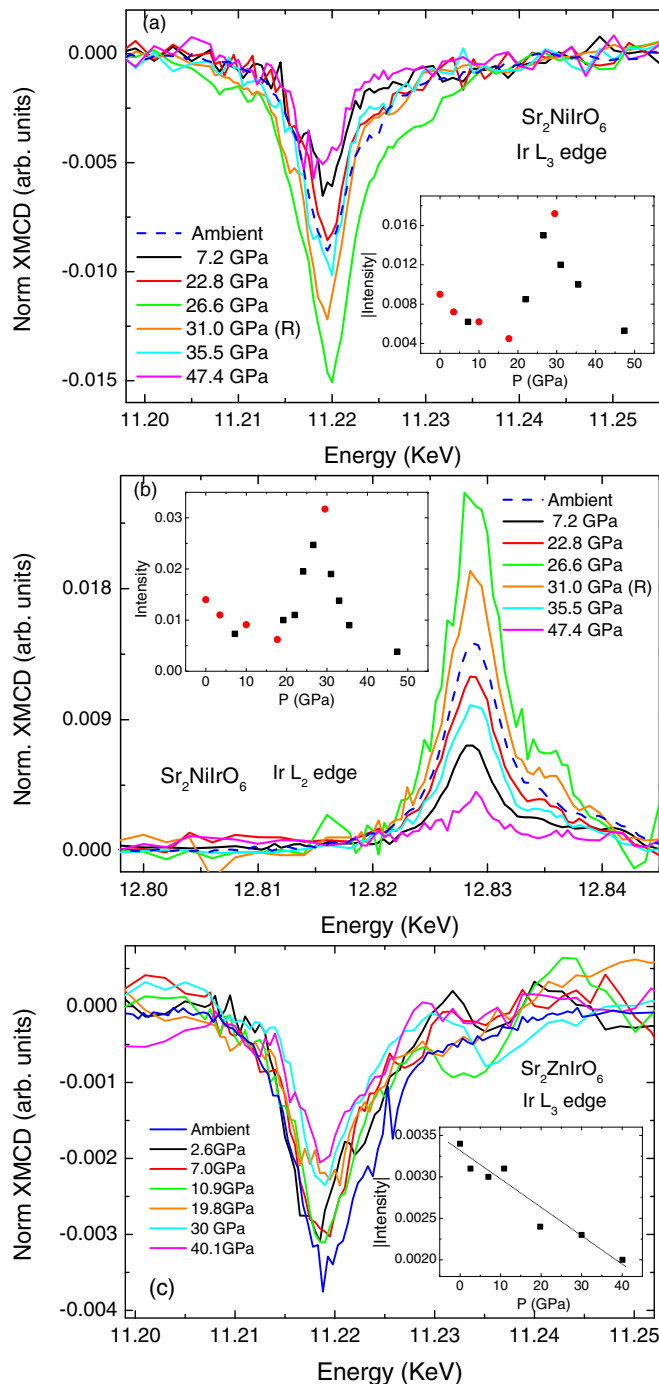
FIG. 1. Pressure dependence of the XMCD spectra recorded at (a) the Ir L_3-edge of Sr_2NiIrO_6, (b) the Ir L_2-edge of Sr_2NiIrO_6, and (c) the Ir L_3-edge of Sr_2ZnIrO_6. For the sake of clarity the XMCD spectra are shown only for selected pressures for Sr_2NiIrO_6 and a smoothing has been applied to the Sr_2ZnIrO_6 data under pressure. The insets show a direct comparison of the modulus of the XMCD intensity for both samples. Different colors correspond to spectra recorded in different times and using different DACs. (R) indicates released pressure.

in the whole pressure range. For a FM structure, on the other hand, an Ir $L_2(L_3)$-edge XMCD intensity of ∼0.9 (0.6) would be expected, based on the data reported on Refs. [19,36]. Therefore, this is indicative of the presence of strong AFM

exchange interactions favoring an arrangement of magnetic moments with nearly zero net magnetization throughout the whole pressure range.

For Sr_2ZnIrO_6, on the other hand, the intensity of the XMCD signal undergoes a slow, gradual reduction, down to a ∼40% decrease at 40 GPa as can be seen in the inset of Fig. 1(c). It can also be observed that the XMCD intensity in Sr_2ZnIrO_6 is smaller than in Sr_2NiIrO_6 in the whole pressure range. Based on the previously reported similar temperature dependence of the magnetic susceptibility [16], one could expect a similar arrangement of magnetic moments in both Sr_2ZnIrO_6 and Sr_2NiIrO_6 compounds. However, the current pressure data suggest, on the contrary, different magnetic structures. This would be in agreement with the dissimilar frustration index for Sr_2ZnIrO_6 ($f_{frus} = 9.5$) and Sr_2NiIrO_6 (1.4), as noted above.

Apart from the overall modulation of the intensity, no change is observed in the XMCD spectral lineshapes recorded on both edges of Sr_2NiIrO_6. Therefore, the amplitude variations of the XMCD spectra can be directly related to the changes of the net Ir sublattice moments.

The XAS spectra (Fig. 2) show very small variations with increasing pressure up to ∼45 GPa. In particular, the white line intensity at the L_3 edge decreases about ∼5% for both samples, i.e., 0.1%/GPa decrease rate. Besides, a small shift of the threshold to higher energies (0.22 eV and 0.35 eV in the case of the Ni and Zn samples, respectively) can be observed. This is most likely related to structural compression [37] rather than to a valence change since in the case of Sr_2ZnIrO_6 a Zn valence above the divalent state seems unrealistic. The structural compression origin is confirmed by the EXAFS data (below). Besides, the splitting between the two minima in the second derivative of the Ir L_3 XANES (inset of Fig. 2) indicates that pressure could also cause an ∼0.9 eV increase of the crystal electric field (CEF) in both samples [36,38,39]. In the case of Sr_2NiIrO_6 the value of the $\langle \mathbf{L} \cdot \mathbf{S} \rangle$ calculated from the branching ratio of the absorption spectra [36,40] remains roughly constant at ∼2.1 up to 47 GPa. This agrees with a pressure-independent character of the atomic magnetic moment (i.e., m_l/m_s) of Ir.

B. Structural characterization

Figure 3 shows XRD patterns at low temperature ($T = 10$ K) for applied pressures up to ∼48 GPa. As hydrostatic pressure is applied the diffraction pattern shifts, indicating a volume reduction. No feature indicative of a structural phase transition was observed in the entire pressure range. Therefore, the monoclinic $P2_1/n$ space group, i.e., that reported for this oxide in the 5- to 100-K temperature range at ambient pressure [16], was used in the fits to obtain the lattice parameters.

Despite the lack of signs of phase transition, the diffraction patterns recorded under pressure present broad peaks and low signal-to-noise ratio in comparison to those recorded at ambient pressure [16]. This broadening suggests a large degree of disorder affecting the position of some atoms, even for the lowest pressure, 2.3 GPa, where no effect of pressure gradient is expected [41,42].
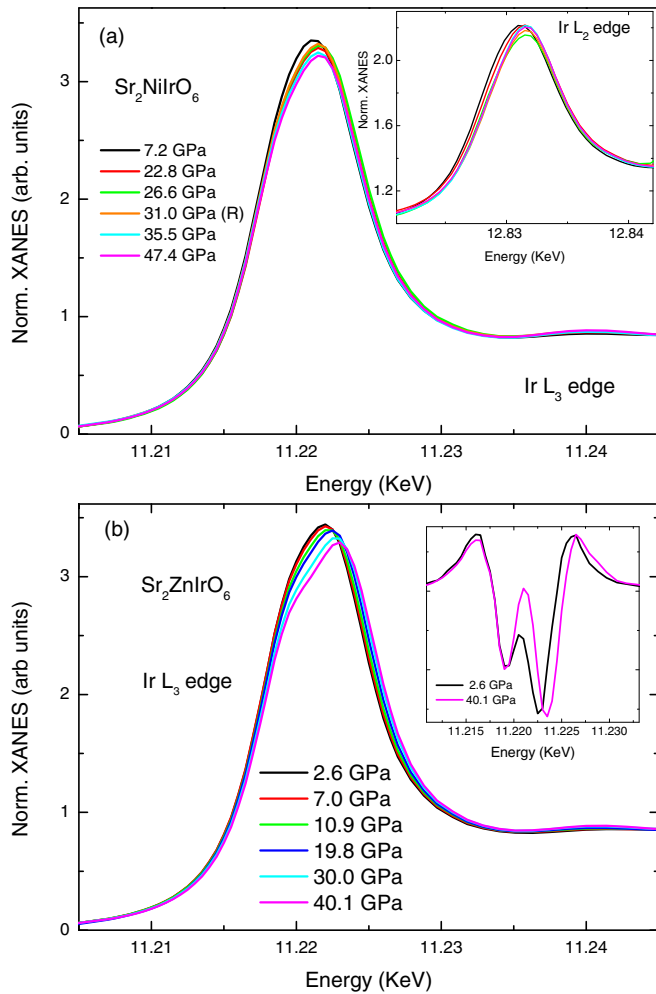
FIG. 2. Pressure dependence of the XAS spectra recorded on Sr_2NiIrO_6 (a) and Sr_2ZnIrO_6 (b). The inset in (a) shows the pressure dependence at the Ir L_2 edge. The inset in (b) shows the second derivative of the XANES recorded at the Ir L_2 edge on Sr_2ZnIrO_6.

Limitations in the extent of powder averaging due to the small focused x-ray beam, peak broadening as a result of pressure gradients in the quasihydrostatic medium, limited angular range, and the presence of ruby and Au pressure markers prevented us from carrying out reliable Rietveld refinements. Instead, a profile matching of the patterns was performed using the FULLPROF code [25]. Profile matching provided reliable lattice parameters but no information about fractional atomic coordinates and occupancy. These were fixed to their ambient pressure values as given in Ref. [16].

As shown in Fig. 4, the applied pressure drives a continuous reduction of the three lattice parameters, the reduction along the c axis ($\sim 0.31\%$/GPa) being about twice faster than along a ($\sim 0.16\%$/GPa) and b ($\sim 0.19\%$/GPa) so that the c/a ratio decreases from 1.406 at ambient pressure to 1.297 at 47.8 GPa. A change of slope is observed at ~ 17 GPa. Apart from that, although no discontinuities in lattice parameters or signatures of a structural phase transition are found, the b/a ratio presents an anomalous dependence on pressure which correlates with the HP-XMCD. It should be noted here that these XRD data do not allow us to rule out subtle changes
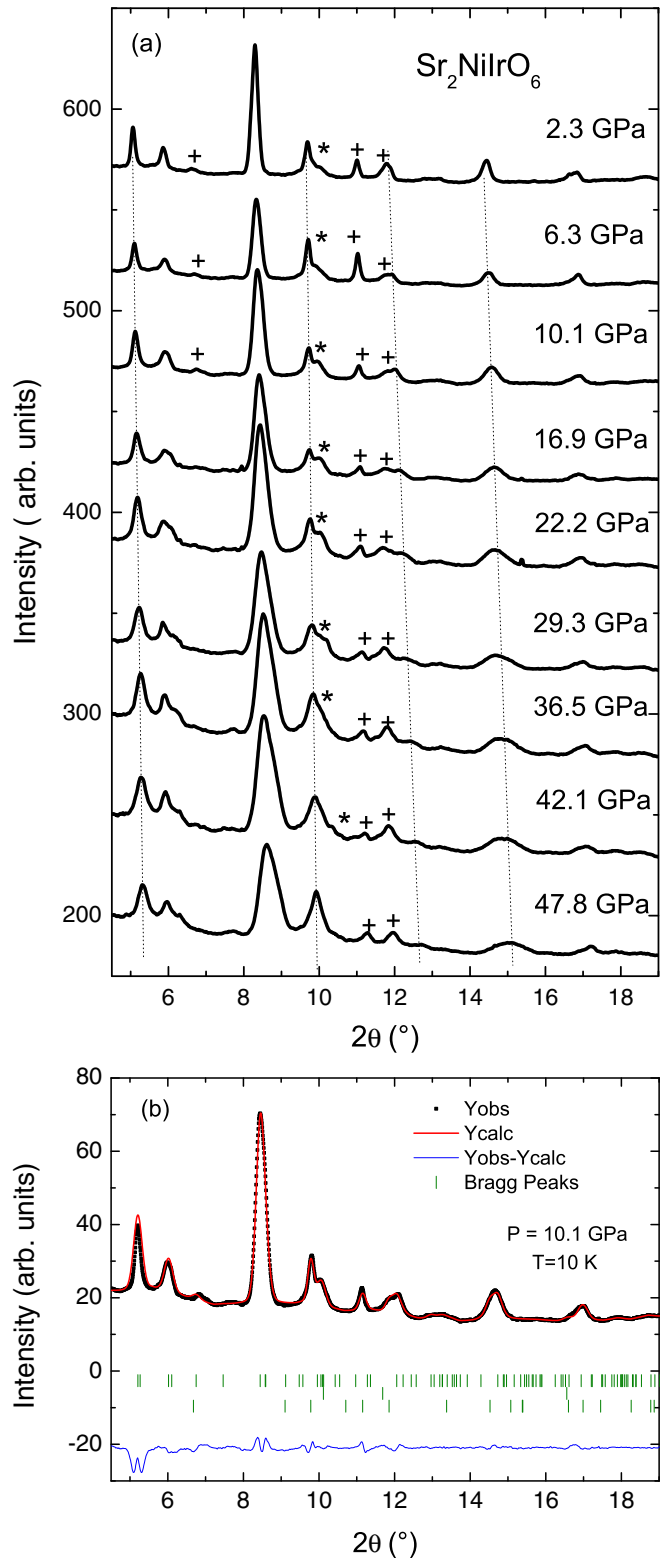

FIG. 3. (a) XRD data collected at $T = 10$ K under different pressures. Dotted lines are guides for the eye showing the shift with increasing pressure for selected reflections. Peaks marked with * and + symbols correspond to Au and ruby markers, respectively. (b) Observed (dots, black) and calculated (red solid line) XRD patterns at 10.1 GPa. The first series of Bragg peaks corresponds to $Sr_2NiIrO_6(P2_1/n)$, the second and third series correspond to Au and ruby.

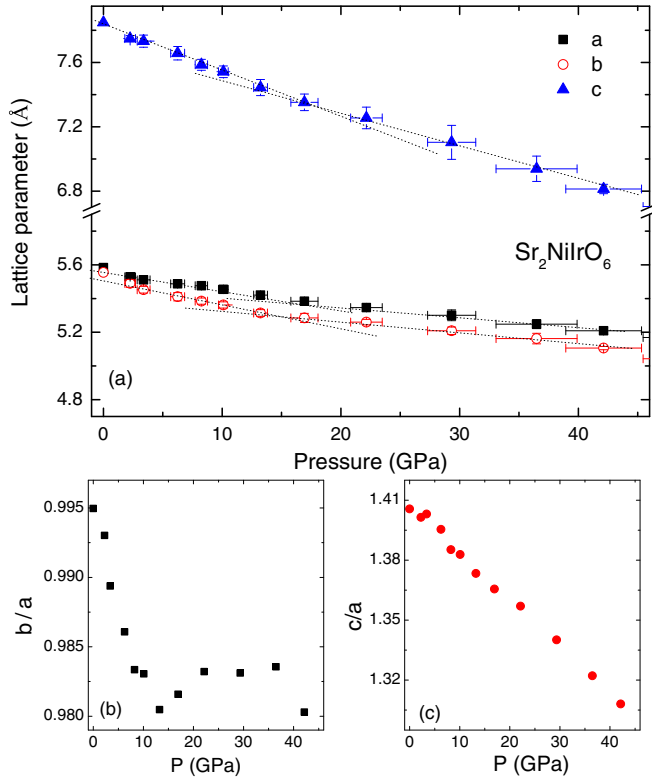FIG. 4. (a) Pressure-dependent lattice parameters for Sr_2NiIrO_6. Dotted lines are guides for the eye. (b) and (c) Shown are the b/a and a/c ratios, respectively.

FIG. 5. Real part of the FTs of the EXAFS signals for the polycrystalline Sr_2NiIrO_6 sample (k range from 2.5 Å^{-1} to 9.4 Å^{-1}; k^2 weighted). The inset shows the modulus of the FT.

in the structure such as small changes in the tilting/rotation angles. In this sense, a modification of the space group from monoclinic P2$_1$/n to triclinic P-1 (with α, $\gamma \neq 0$) cannot be discarded. Nevertheless, attempts to fit the data with the P-1 group neither improve the fits nor reveal discontinuities in the lattice parameters or signatures of a structural phase transition.

To get further insight into the structural changes, EXAFS spectra were also recorded at 10 K and under hydrostatic applied pressure up to 50 GPa. As shown in the Fourier transform (FT) of the EXAFS signals in Fig. 5, the changes from 2.5 GPa to 50 GPa are small and consist mainly on a gradual shift of the FT. All the observed changes are subtle
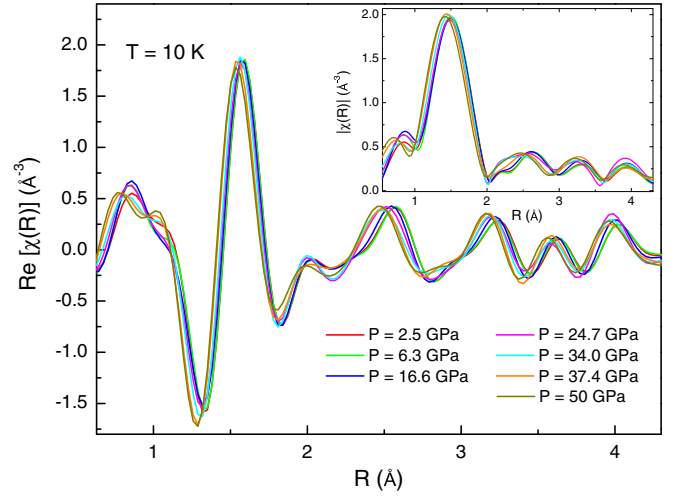
and follow a monotonic evolution along the whole pressure range. In order to correlate the spectral features with specific structural changes, the experimental data have been fitted to a simplified model that includes the contributions to the EXAFS signal coming from five single scattering (SS) paths up to 4.6 Å (that is, O, Sr, Ni, O, and O coordination shells around the absorbing Ir, Ir$_{abs}$) as well as the collinear, focusing multiple scattering (MS) paths involving the same atoms from which the SS occurs (i.e., O-Ir$_{abs}$-O-Ir$_{abs}$, Ni-O-Ir$_{abs}$, and O-Ni-O-Ir$_{abs}$ scattering paths). Each coordination shell has one unique average distance (R_j) and one Debye-Waller (DW) factor. The R_j lengths and DW factors of the MS paths are parametrized in terms of the SS paths in a similar manner to that described in Refs. [43,44], but the Ir-O-Ni angle in our case remains fixed to 180°. The best fit values are summarized in Table I. Attempts to fit the data with a larger number of coordination shells (subshells) and/or using 165° for the Ni-O-Ir angle [16] gave a similar evolution of the fitting parameters with pressure. The large values of σ_3^2 are partially due to the use of perfect collinear MS paths in the model. Using noncollinear paths (165°) reduce σ_3^2 by a factor of ∼2.5, but do not affect

TABLE I. Values of the best fit structural parameters: half path lengths R_j (in Å) and Debye-Waller factors σ^2 (in Å^2) for the Sr_2NiIrO_6 sample. The number of atoms at mean distances R_j around the absorbing atom (N_j) are fixed in the model. $S_0^2 = 0.762$ and $\Delta E_0(eV) = 5.67$ have been fixed to the values obtained for the lowest pressure. The same parameters were used to fit the two distant oxygen shells. The R factor, which is a measure of the misfit between the data and theory, is in the 0.022–0.028 range.

	2.5 GPa	6.3 GPa	16.6 GPa	24.7 GPa	34.0 GPa	37.4 GPa	50.0 GPa
R_1 ⟨Ir-O⟩	1.903(6)	1.903(6)	1.893(6)	1.885(7)	1.881(6)	1.866(6)	1.863(6)
R_2 ⟨Ir-Sr⟩	3.231(50)	3.237(50)	3.212(54)	3.181(64)	3.142(52)	3.139(47)	3.121(45)
R_3 ⟨Ir-Ni⟩	3.910(65)	3.907(67)	3.882(58)	3.853(64)	3.834(61)	3.831(47)	3.819(47)
R_4 ⟨Ir-O⟩	4.324(45)	4.323(45)	4.296(46)	4.257(44)	4.261(55)	4.255(51)	4.241(44)
R_{4b} ⟨Ir-O⟩	4.501(45)	4.500(45)	4.472(46)	4.434(44)	4.437(55)	4.431(51)	4.417(44)
σ_1^2	0.0032(9)	0.0032(9)	0.0037(10)	0.0038(10)	0.0033(10)	0.0037(9)	0.0039(10)
σ_2^2	0.0182(66)	0.0178(67)	0.0178(69)	0.0192(80)	0.0179(67)	0.0178(61)	0.0177(62)
σ_3^2	0.0204(66)	0.0204(67)	0.0178(69)	0.0187(80)	0.0189(67)	0.0169(61)	0.0172(62)
σ_4^2	0.0073(67)	0.0066(64)	0.0063(63)	0.0059(60)	0.0089(87)	0.0092(82)	0.0072(65)

the observed effect of pressure. Similarly, the same trends, although with slightly different values, are obtained regardless of whether ΔE_0 is a free parameter or set to a fixed value for all the pressures. It is to be noted that the limited k-range results in a spatial resolution of $\sim$0.16 Å that does not allow one to resolve small splittings.

The results of the fits indicate a small and gradual shrinkage of both the Ir-O bond distance from 1.903 Å to 1.863 Å ($\sim$0.04%/GPa) and the Ir-Ni bond distance from 3.910 Å to 3.819 Å ($\sim$0.05%/GPa) in the 2- to 50-GPa range. From these values no abrupt or nonmonotonic structural change can be inferred that can explain the evolution of the XMCD with pressure. Similarly, the DW factors do not show any abrupt modification that can be directly correlated to the pressure dependence of the XMCD signal. The DW factors do not show a clear decrease under pressure. This may be indicative of disorder, which is consistent with the XRD peak broadening observed at relatively low pressure. This pressure-induced disorder would not be related to the occupancies at A, B, and B' sites on the $A_2BB'O_2$ structure but to structural disorder associated with distortions of the IrO_6 octahedra and changes in the Ir-O-Ni bond angles.

C. Discussion

First, it should be noted that, contrary to the high degree of tunability of other $3d$-$5d$ double perovskites [11], the magnetization of Sr_2NiIrO_6 is robust and not largely affected by hydrostatic pressure. Even when the intensity of the XMCD at 30 GPa reaches twice its ambient pressure value, the signal is very small for the whole pressure range up to $\sim$45 GPa. In fact, the maximum intensity observed at the L_2 edge (0.0245) remains very far from the 0.6–0.9 expected for a FM Ir sublattice, indicating the important role of long-range AFM Ir-Ir interactions. This can also be inferred from the Sr_2ZnIrO_6 data, where 40 GPa causes a reduction of only 40% of the XMCD intensity. Besides, the small change of the XMCD in Sr_2NiIrO_6 suggests that either the strength of both interactions, FM Ir-Ni and AFM Ir-Ir, is affected in a similar manner or both are only very slightly modified in the range of 0–45 GPa. In this sense, the fact that the initial (at ambient) Ir-O-Ni angles are not perfectly collinear but 165.6°, 170.2°, and 163.7° could be a key factor since the FM Ir-Ni coupling is already weakened at ambient pressure due to the buckling of these bonds.

Despite the above discussion, the pressure dependence of XMCD is found to be remarkably different for Sr_2NiIrO_6 and Sr_2ZnIrO_6 samples. This is indicative of the important role played by the Ir-Ni interactions and the different magnetic arrangement in both samples. In the Sr_2NiIrO_6 sample this arrangement has been reported to consist of a complex helical magnetic structure with an incommensurate propagation vector of $(0,k,k)$ with $k = 0.35591$ and relative phase ϕ on each sublattice [15] (see Fig. 6). What drives the puzzling pressure dependence of the XMCD signal of the Sr_2NiIrO_6 sample? A possible origin for the change of the magnetic structure is related to the pressure-driven modification of the CEF. For example, for Sr_2FeOsO_6 it has been proposed that upon lattice compression the CEFs at $3d$ and $5d$ sites become more disparate and there is a weakening of the FM
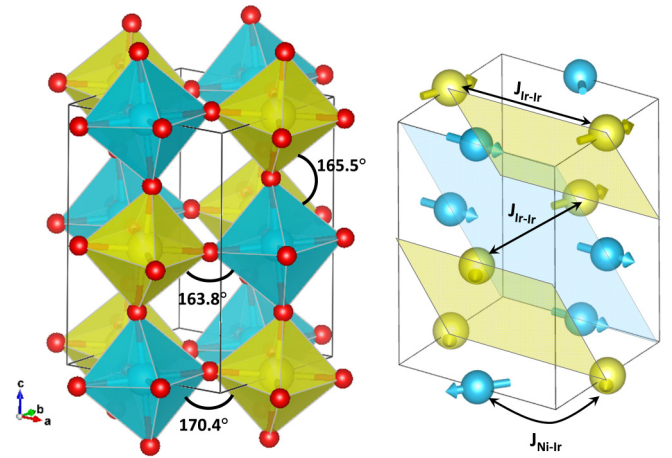

FIG. 6. (Left) Sketch of the crystal structure including the octahedral tilts [45]. (Right) Sketch of the magnetic structure including the semitransparent FM planes normal to the $(0,k,k)$ magnetic propagation vector.

Fe(e_g)-Os(e_g) interaction relative to the AFM Fe(t_{2g})-Os(t_{2g}) interaction [11]. In the case of Sr_2NiIrO_6, the evolution of R_1 ⟨Ir-O⟩ and σ_1^2 in Table I indicates a compression and a slight distortion of the IrO_6 octahedra with HP. The reduction of the Ir-O bond length in turn causes an $\sim$0.9-eV increase of the CEF, that could affect the Ir-Ni exchange interaction. However, contrary to the Fe-Os case, for $\sim$180° bonding, any electron hopping here is expected to give FM coupling between the Ni^{2+} ($t_{2g}^6 e_g^2$) and Ir^{6+} (t_{2g}^3) ions [14]. Moreover, according to the second derivative of the XAS spectra the modification of the CEF is gradual with pressure, so it can hardly explain the nonmonotonic pressure dependence of the XMCD spectra.

As seen in the EXAFS section, no abrupt or discontinuous structural modification is observed in the Ir-Ni distances with increasing pressure so the nonmonotonic variation of XMCD cannot be explained in terms of a nonmonotonic change in the Ir-Ni distance as one might naively expect. In addition, in contrast to the most common scenario for double perovskites, Sr_2NiIrO_6 presents a complex helical magnetic structure that hampers identifying a direct relationship between the magnetic structure and the Ir-O-Ni bucklings. Consequently, no direct relationship can be established between the evolution of the XMCD and a specific change of the Ir-O-Ni bucklings. It should be noted, however, that the presence of very subtle or complex changes in the Ir-Ni distances and/or Ir-O-Ni buckling angles, undetected by our EXAFS probe, cannot be ruled out.

On the other hand, the b/a ratio changes nonmonotonically and its pressure dependence can be correlated with the XMCD evolution. Indeed, the increase/decrease of the XMCD signal is concomitant with an increase/decrease of the b/a ratio, which gets lower in the ranges of 0–13 GPa and 36–46 GPa but presents a slight increase (from 0.980 to 0.983) in the range of 13–36 GPa. Moreover, the change of slope observed in a, b, and c in Fig. 4 is coinciding with the rise of the XMCD signal. It is seen, therefore, that the structure reflects the magnetic changes with pressure, as one could expect in an iridate with extended $5d$ orbitals. While a fully definite relationship

between structure and magnetism remains elusive, the concurrent evolution of the XMCD intensity and the b/a ratio allows us to get an insight into the evolution of the magnetic interactions. Given the lack of uncompensated moment in zero field [16], the XMCD directly reflects the canting of the moments induced by the applied field [16], so a higher intensity of the XMCD indicates a weaker AFM interaction. In other words, increasing the b/a ratio from 0.980 to 0.984, i.e., reducing the difference between these two lattice parameters, results in a weakening of the AFM interaction between the FM planes. Reducing the b/a ratio, on the other hand, results in a stronger AFM interaction between the FM planes. Besides, it is to be noted that the helical structure observed at ambient pressure presents FM Ir-Ir (and Ni-Ni) alignment along the longer a axis and AFM (with $\phi \sim 128°$) alignment along the shorter b axis. Further reducing (increasing) the length of b relative to a with pressure, seems to further stabilize (destabilize) the helical structure observed at ambient pressure. Following a similar argument it can be assumed that the decrease of the c/a ratio also contributes to stabilizing the helical structure and increases the relative strength of the AFM interaction. Overall, therefore, we interpret the nonmonotonic evolution of the XMCD as arising from subtle changes in the magnetic anisotropy related to the b/a ratio and allowing more (less) field-induced canting. The weakening of the long-range Ir-Ir antiferromagnetic exchange interactions is likely concomitant with a change of the incommensurate wave vector k. While the precise change of the magnetic structure with pressure has yet to be probed, the XMCD clearly indicates that the weakening of the AFM Ir-Ir interactions is not enough to give rise to a ferromagnetic or ferrimagnetic arrangement.

Finally, it should be noted that in Sr_2NiIrO_6 none of the initial (i.e., measured at ambient pressure) Ir-O-Ni angles are perfectly collinear but 165.6°, 170.2°, and 163.7°. This is likely an important factor determining the low tunability of Sr_2NiIrO_6 with HP. Chemical pressure, on the other hand, $Sr_{2-x}Ca_xNiIrO_6$ or $Sr_{2-x}Ba_xNiIrO_6$, could result in lower ($\sim150°$) or higher ($\sim180°$) angles, respectively. This could provide a more effective route to change the strength of the exchange interactions and tune the magnetic ground state. Unfortunately, however, initial attempts to prepare single-phase doped samples to study the effect of chemical pressure have been unsuccessful to date. The results so far indicate that very high pressure synthesis conditions will be required to stabilize these compounds.

IV. SUMMARY AND CONCLUSIONS

Prompted by the unexpected AFM behavior of the Sr_2NiIrO_6 double perovskite and the theoretical works reporting that the long-range AFM Ir-Ir interaction overwhelms the first nearest neighbor FM Ir-Ni interaction, we have explored the tunability of the magnetic structure with hydrostatic pressure. The fact that the magnetic structure in Sr_2NiIrO_6 is helical means that both AFM and FM are at play in this oxide. The important role of both interactions is confirmed by the dissimilar response of Sr_2NiIrO_6 and Sr_2ZnIrO_6 to HP, indicating that the magnetic structure in these two compounds is different despite the similar M(H) behavior. In Sr_2NiIrO_6, the XMCD reveals a puzzling nonmonotonic dependence on pressure. An origin based on the modification of the CEFs with pressure has been discarded. The complex helical magnetic structure hampers an understanding of the magnetic structure in terms of bond angles. On the other hand, we have found that the nonmonotonic evolution of the XMCD signal appears to be correlated with nonmonotonic changes in the b/a ratio. As the length of the b lattice parameter gets closer to (further from) a, the AFM Ir-Ir interaction strength decrease (increases) enabling a larger (smaller) canting of magnetic moments along the applied field with commensurate changes in the XMCD signal. This, however, is not enough to make the Sr_2NiIrO_6 a ferromagnet or ferrimagnet. Chemical pressure is expected to have a larger effect on the bonding Ni-O-Ir angles and so it might be a more effective route to tune the magnetic structure, allowing a FM alignment of the Ir ions. Further experiments (such as resonant magnetic scattering under pressure [46]) are needed to figure out the actual changes in the magnetic structure that give rise to the interesting changes observed in the XMCD of Sr_2NiIrO_6 under pressure.

[1] W. Witczak-Krempa, G. Chen, Y. B. Kim, and L. Balents, Annu. Rev. Condens. Matter Phys. **5**, 57 (2014).

[2] J. G. Rau, E. K.-H. Lee, and H.-Y. Kee, Annu. Rev. Condens. Matter Phys. **7**, 195 (2016).

[3] G. Cao and P. Schlottmann, Rep. Prog. Phys. **81**, 042502 (2018).

[4] T. K. Mandal, C. Felser, M. Greenblatt, and J. Kübler, Phys. Rev. B **78**, 134431 (2008).

[5] C. A. Escanhoela, G. Fabbris, F. Sun, C. Park, J. Gopalakrishnan, K. Ramesha, E. Granado, N. M. Souza-Neto, M. van Veenendaal, and D. Haskel, Phys. Rev. B **98**, 054402 (2018).

[6] P. Majewskia, S. Geprags, O. Sanganas, M. Opel, R. Gross, F. Wilhelm, A. Rogalev, and L. Alff, Appl. Phys. Lett. **87**, 202503 (2005).

[7] H. Wu, Phys. Rev. B **64**, 125126 (2001).

[8] E. Arias-Egido, M. Laguna-Marco, C. Piquer, J. Chaboy, G. Fabbris, and D. Haskel, Mater. Des. **196**, 109083 (2020).

[9] J. B. Goodenough, Phys. Rev. **100**, 564 (1955).

[10] J. Kanamori, J. Phys. Chem. Solids **10**, 87 (1959).

[11] L. S. I. Veiga, G. Fabbris, M. van Veenendaal, N. M. Souza-Neto, H. L. Feng, K. Yamaura, and D. Haskel, Phys. Rev. B **91**, 235135 (2015).

[12] R. Morrow, K. Samanta, T. S. Dasgupta, J. Xiong, J. W. Freeland, D. Haskel, and P. M. Woodward, Chem. Mater. **28**, 3666 (2016).

[13] R. Morrow, J. W. Freeland, and P. M. Woodward, Inorg. Chem. **53**, 7983 (2014).

[14] X. Ou, Z. Li, F. Fan, H. Wang, and H. Wu, Sci. Rep. **4**, 7542 (2014).

[15] K. Rolfs, S. Tóth, E. Pomjakushina, D. T. Adroja, D. Khalyavin, and K. Conder, Phys. Rev. B **95**, 140403(R) (2017).

[16] P. Kayser, M. J. Martinez-Lope, J. A. Alonso, M. Retuerto, M. Croft, A. Ignatov, and M. T. Fernandez-Diaz, Inorg. Chem. **52**, 11013 (2013).

[17] N. Narayanan, D. Mikhailova, A. Senyshyn, D. M. Trots, R. Laskowski, P. Blaha, K. Schwarz, H. Fuess, and H. Ehrenberg, Phys. Rev. B **82**, 024403 (2010).

[18] A. Kolchinskaya, P. Komissinskiy, M. B. Yazdi, M. Vafaee, D. Mikhailova, N. Narayanan, H. Ehrenberg, F. Wilhelm, A. Rogalev, and L. Alff, Phys. Rev. B **85**, 224422 (2012).

[19] P. Kayser, M. J. Martinez-Lope, J. A. Alonso, M. Retuerto, M. Croft, A. Ignatov, and M. T. Fernandez-Diaz, Eur. J. Inorg. Chem. **2014**, 178 (2014).

[20] D. Harada, M. Wakeshima, Y. Hinatsu, K. Ohoyama, and Y. Yamaguchi, J. Phys.: Condens. Matter **12**, 3229 (2000).

[21] S. Agrestini, K. Chen, C. Y. Kuo, L. Zhao, H. J. Lin, C. T. Chen, A. Rogalev, P. Ohresser, T. S. Chan, S. C. Weng, G. Auffermann, A. Volzke, A. C. Komarek, K. Yamaura, M. W. Haverkort, Z. Hu, and L. H. Tjeng, Phys. Rev. B **100**, 014443 (2019).

[22] J. Flynn, J. Li, A. P. Ramirez, and M. Subramanian, J. Solid State Chem. **247**, 53 (2017).

[23] W. Kockelmann, D. Adroja, A. Hillier, M. Wakeshima, Y. Izumiyama, Y. Hinatsu, K. Knight, D. Visser, and B. Rainford, Phys. B: Condens. Matter **378**, 543 (2006).

[24] C. Prescher and V. B. Prakapenka, High Press. Res. **35**, 223 (2015).

[25] J. Rodriguez-Carvajal, Phys. B: Condens. Matter **192**, 55 (1993).

[26] S. Pascarelli, O. Mathon, T. Mairs, I. Kantor, G. Agostini, C. Strohm, S. Pasternak, F. Perrin, G. Berruyer, P. Chappelet *et al.*, J. Synchrotron Rad. **23**, 353 (2016).

[27] T. Irifune, A. Kurio, S. Sakamoto, T. Inoue, and H. Sumiya, Nature **421**, 599 (2003).

[28] D. E. Sayers and B. Bunker, in *X-Ray Absorption: Principles, Applications, Techniques of EXAFS, SEXAFS, and XANES* (Wiley, New York, 1988), Chap. 6.

[29] M. Newville, J. Synchrotron Rad. **8**, 322 (2001).

[30] B. Ravel and M. Newville, J. Synchrotron Rad. **12**, 537 (2005).

[31] J. J. Rehr, J. J. Kas, M. P. Prange, A. P. Sorini, Y. Takimoto, and F. Vila, C. R. Phys. **10**, 548 (2009).

[32] K. Hirano, K. Izumi, T. Ishikawa, S. Annaka, and S. Kikuta, Jpn. J. Appl. Phys. **30**, L407 (1991).

[33] J. C. Lang and G. Srajer, Rev. Sci. Instrum. **66**, 1540 (1995).

[34] M. Suzuki, N. Kawamura, M. Mizumaki, A. Urta, H. Maruyama, S. Goto, and T. Ishikawa, Jpn. J. Appl. Phys. **37**, L1488 (1998).

[35] D. Haskel, Y. C. Tseng, N. M. Souza-Neto, J. C. Lang, S. Sinogeikin, Y. Mudryk, V. K. Pecharsky, and K. A. Gschneidner, Jr., High Press. Res. **28**, 185 (2008).

[36] M. A. Laguna-Marco, P. Kayser, J. A. Alonso, M. J. Martinez-Lope, M. van Veenendaal, Y. Choi, and D. Haskel, Phys. Rev. B **91**, 214433 (2015).

[37] J. Chaboy, J. Synchrotron Rad **16**, 533 (2009).

[38] J.-H. Choy, D.-K. Kim, G. Demazeau, and D.-Y. Jung, J. Phys. Chem. **98**, 6258 (1994).

[39] J.-H. Choy, D.-K. Kim, S.-H. Hwang, G. Demazeau, and D.-Y. Jung, J. Am. Chem. Soc **117**, 8557 (1995).

[40] G. van der Laan and B. T. Thole, Phys. Rev. Lett. **60**, 1977 (1988).

[41] N. Tateiwa and Y. Haga, J. Phys.: Conf. Ser. **215**, 012178 (2010).

[42] Y. Feng, R. Jaramillo, J. Wang, Y. Ren, and T. F. Rosenbaum, Rev Sci Instrum. **81**, 041301 (2010).

[43] D. Haskel, E. A. Stern, F. Dogan, and A. R. Moodenbaugh, Phys. Rev. B **61**, 7055 (2000).

[44] D. Haskel, Ph.D thesis, University of Washington, 1998.

[45] K. Momma and F. Izumi, J. Appl. Crystallogr. **44**, 1272 (2011).

[46] D. Haskel, G. Fabbris, J. H. Kim, L. S. I. Veiga, J. R. L. Mardegan, C. A. Escanhoela, S. Chikara, V. Struzhkin, T. Senthil, B. J. Kim, G. Cao, and J. W. Kim, Phys. Rev. Lett. **124**, 067201 (2020).